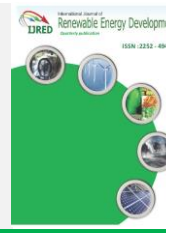




Contents list available at IJRED website

International Journal of Renewable Energy Development

Journal homepage: <https://ijred.undip.ac.id>



Research Article

Experimental Evaluation of Thermohydraulic Performance of Tubular Solar Air Heater

Yousif Fateh Midhat* and Issam Mohammed Ali Aljubury

Mechanical Engineering Department, College of Engineering, Baghdad, University of Baghdad, Iraq

Abstract. The thermohydraulic performance of a new design solar air heater (SAH) design was examined experimentally in this paper as a trial to improve the flat-plate SAH's efficiency. A flat-plate solar air heater (FPSAH) and a jacketed tubular solar air heater (JTSAH) having similar dimensions were constructed to compare their thermal performance efficiencies. A band of Aluminum jacketed tubes were arranged side by side in parallel to the airflow direction to form the absorber of a jacketed tubular solar air heater (JTSAH). The experiments were accomplished at three mass flow rates (MFR)s: 0.011 kg/s, 0.033 kg/s, and 0.055 kg/s. Results revealed that the maximum temperature difference was obtained from JTSAH at 38°C in comparison to 32°C from the FPSAH at MFR of 0.011 kg/s. The thermal losses from the upper glass cover of the JTSAH were less than the same losses at the FPSAH due to the reduced absorber and glass temperatures of the JTSAH. The gained power was higher at the JTSAH than the FPSAH. At the JTSAH, at 0.055 kg/s MFR, the maximum average thermal efficiency obtained was 81%, and the maximum average thermos-hydraulic efficiency obtained was 75.61 %. It is noted that increasing the MFR increases the thermal efficiency, also, its optimum value rises the thermos-hydraulic efficiency to a specific optimum point. The pressure drop increases with the MFR and JTSAH compared to the FPSAH.

Keywords: Solar Air Heater, Tubular, Flat, Absorber, glass cover.



@ The author(s). Published by CBIORE. This is an open access article under the CC BY-SA license (<http://creativecommons.org/licenses/by-sa/4.0/>)

Received: 20th March 2022; Revised: 6th July 2022; Accepted: 26th Sept 2022; Available online: 10th Oct 2022

1 Introduction

Energy is a crucial need that touches the civilized life on earth, so humans worked to get it in many ways. The growing energy difficulties, decreasing fossil energy funds, and massive environmental problems led to enormous attention on green energy sources. Fossil fuels are limited and depleted continuously, and it is necessary to save some of the fossil fuels to conserve for upcoming generations. Energy problems forced nations to use renewable energy resources like wind and sun to substitute for fossil fuels (Soares, 2015).

Today, solar energy is well-intended because of its availability, cost-benefit, effectiveness, and sustainability in reducing carbon and poisonous gasses. Solar air heater (SAH) is an initial application that uses solar energy to absorb the energy irradiated on it (Singh Patel & Lanjewar, 2019). Solar energy absorption using SAH is a promising technology that makes use of solar energy. SAH is a setup used to heat air used in many applications like domestic heating, industrial processes, desalination of hard water, residential air conditioning, dehydration of agricultural products, greenhouses, electricity generation, and space heating (Bakry *et al.*, 2018). SAH has a simple structure, reliable, stable, has low installation costs, and is easy to maintain (Chabane *et al.*, 2014). The performance of SAH is affected negatively by many factors like the low conductivity, the low thermal capacity of air, and the absorber area. Furthermore, other factors can limit this efficiency, like the

reflected, convected, and radiated heat through the parts of SAH as heat losses (Hassan & Abo-Elfadl, 2018). To enhance the thermal performance of SAH, innovative attempts had been employed, as detailed in the following review listed in chronological order. An investigation of the performance of a SAH combined with a microjet was studied by Zukowski, (2015), the setup's efficiency reached about 90%. Dissa *et al.*, (2016) enhanced the efficiency of a SAH experimentally by using an absorber plate composed of a coupling of a corrugated plate and porous medium, the efficiency enhancement of the SAH was 6%. (Ravi & Saini, 2016) used discrete V-ribs to enhance the smooth absorber SAH's heat transfer, they increased Nusselt number to 450 compared to a smooth absorber of 120. The performance of a circular cross-section SAH was studied by Abdullah *et al.*, (2017), the absorber was constructed from a half of circle, while the glass represented the second part of the section. The maximum efficiency of the SAH was 80%. Aboghrara *et al.*, (2017) used jet impingement to increase the thermal efficiency of a SAH; it increased from 53% at a flat absorber to 68% at a corrugated absorber. Abdullah *et al.*, (2018) investigated solar air heater's efficiency without and with turbulence obstacles using thin cans, the result was improving the SAH's thermal efficiency from 38% to 70 %, respectively. The performance of a curved SAH using CFD software was studied by (Singh & Singh, 2018) and they found a rise in the outlet air temperature to 70°C in the case of a curved plate design of a single pass V-tubulated SAH

* Corresponding author

Email: yousif.midhat1403m@coeng.uobaghdad.edu.iq (Y.F. Midhat)

design. Heydari & Mesgarpour, (2018) investigated a SAH's design of a helical channel, they found that the SAH has higher thermal efficiency with 14% larger than the double pass without a helical channel. An experimental work investigated a SAH's thermal performance by (Saravanakumar *et al.*, 2019) to increase the efficiency by attaching arc-ribs and baffles on the absorber plate, the results showed an increase in the energy efficiency and effectiveness by 28.3% and 27.1%, more than the case without baffles and fins. Komolafe *et al.*, (2019) designed a SAH combined with rectangular ribs installed on the absorber plate, they found that the thermal efficiency was close to 56.5%, with an average of 30%. (Wang *et al.*, 2019) studied the performance of a spiral SAH, the average efficiency was 60%, with a 7% increment than the efficiency of SAH with a serpentine absorber. (Jouybari & Lundström, 2020) increased SAH's thermohydraulic parameter from 3.74 to 5.5 by covering the absorber with a porous matrix material. (Yagnesh Sharma *et al.*, 2019) employed an absorber plate with turbulators to get a higher heat transfer coefficient and increase the Nusselt number more considerably than the absorber without turbulators. (Hosseini *et al.*, 2019) investigated a finned absorber's efficiency with variant shapes, flow rates, and inclination angles; the rectangular finned absorber gave a maximum efficiency of 66% with an increment of 10% using a triangular fin. Fiuk & Dutkowski, (2019) fabricated two SAHs, the first with a flat absorber and the second with a wavy absorber to compare their efficiencies, the two SAHs efficiencies were 45% and 74%, respectively. Wang *et al.*, (2020) attached "S" shaped ribs with a gap, they studied the effect of rib spacing, rib width, airflow, and channel height on the efficiency of SAH, the findings indicated an increase in efficiency from 12% to 49% under specified conditions related to the flat SAH one. Bensaci *et al.*, (2020) examined numerically and experimentally baffles arrangement along with the absorber and their effect on the efficiency of SAH, the case of 100% baffled absorber gives the maximum efficiency of 90% with an outlet temperature of 75°C. Sivakandhan *et al.*, (2020) used inclined ribs on a flat absorber of a parallel pass SAH, the ribs improved the thermal efficiency by 22.4% compared to conventional parallel pass SAH. Also, they initiated that maximum efficiency of 80% can be attained under the conditions of the experiment. Nidhul *et al.*, (2020) used a V-ribbed absorber to get energetic efficiency of 23%, effectiveness factor of 2, and exergetic efficiency of 2.5%, with an increment of 0.5% than smooth absorber at an inclination angle of rib 45°. An experimental test used single and double pass serpentine wavy wire-mesh bed SAH by Singh (Singh, 2020), concluded that the studied SAH's thermohydraulic efficiency is about 75% in comparison to a single pass of efficiency 67%. The efficiency of a modified SAH by combining it with a heat storage part consisting of copper tubes filled with thermal storage fluid studied by Kalaiarasi *et al.*, the modified SAH's average efficiency tended to be 67% in comparison to 40% for the same experiment without heat storage material at a flow rate of 0.027 kg/s (Kalaiarasi *et al.*, 2020). Shetty *et al.*, (2020) studied the performance of a SAH with a circular-shape absorber, the perforation holes' diameter and number affected the performance of the SAH, the results showed that the proposed design was the highest in thermal efficiency of 93% compared to 70% for conventional SAH. Ghrilahre *et al.*, (2020) enhanced a SAH's thermal efficiency using arc-ribs attached to the flat absorber, the investigation showed that the highest thermal efficiency for downstream and upstream flow arrangements is 69% and 73% correspondingly. The performance of a tubular SAH with fins was studied experimentally by Murali *et al.*, (2020), the maximum efficiency of SAH reaches 70 % and 65% with and without fins, respectively, at 0.045 kg/s air flowrate.

In the light of the previous review and author surveys, despite many trials to enhance the thermal performance of SAH

by many researchers last years, efforts are still required to enhance the SAH's performance (outlet air temperature, thermal energy gain, and efficiency). Modifying the SAH's absorber is a means of increasing its performance. The absorber's design of any SAH has been the subject of many experimental investigations and studies.

Researchers concluded that the obstacles geometries attached to the flat absorber or extruded from it may enhance the SAH's performance, but, eddies get entrapped in upstream and downstream corners, leading to the formation of local hotspots (Arunkumar *et al.*, 2020; Thakur *et al.*, 2017), or increasing pressure drop, and increased air blowing power (Chand & Chand, 2018).

The objective of present study is to enhance experimentally the thermos-hydraulic performance of a SAH by suggesting a more effective absorber surface with a reasonably low-pressure drop, increasing the heat transfer and low manufacturing cost. The effect of a jacketed tube absorber on SAH's performance had not been investigated yet, it has many main advantages, like: the larger contact area with air over the flat-plate absorber, no entrapped eddies, and the low-pressure drop, these advantages may result in better thermohydraulic performance. In the current experimental study, two SAHs were designed and built, the first one had a flat-plate absorber (FPSAH), and the second had a tubular absorber (J TSAH). The J TSAH's performance was investigated, and its operating parameters were compared with the FPSAH. The investigation is established at three air mass flow rates (MFRs) of 0.011, 0.033, and 0.055 kg/s for the two SAHs. This research is an attempt to resolve the issue of the FPSAH's low thermos-hydraulic efficiency.

2 Materials and Methods

Two similar SAHs except for their absorber surfaces as shown in Fig 1 have been designed and fabricated with the same dimensions, and materials, the first one is a flat plate SAH of lower flow as shown in Fig 2 and Fig 4 (a), and the other is a tubular SAH with a tubular absorber as shown in Fig 3 and Fig 4 (b). The setup is installed in Baghdad city (latitude 33.3152° N and longitude angle 44.3661° E). Air flows through the lower side of the FPSAH flat plate, as shown in Fig 2, so the flow is (lower flow). The dimensions of the flat absorber are 68 cm × 150 cm. Dimensions in all figures are in (cm) units. The tubular absorber is constructed from circular tubes, each tube has two lateral jackets around the inner tube.

In other words, each tube is double in diameter; the external tube has two confronted grooves of 1 cm width to form two lateral jackets from the external diameter, each tube is 150 cm in length, 1.5 cm inner diameter, and external diameter of 4 cm.



Fig 1. The experimental setup

The tubular absorber is shown in Fig 3 and Fig 4. Each tube is fixed by a screw and a washer on the upper and lower edge. Both of the absorbers are centered between the glass cover and the lower side. The projected area of the tubular absorber is the same as the flat absorber. The two absorbers are dyed with black paint to increase their absorptivity of solar irradiation. Air is induced through the inlet port of the SAH and out through the outlet port. As shown in Fig 3. A cross-flow blower is attached to the outlet port of each SAH to induce air into each SAH. The purpose of using such type of blower is to ensure a uniform airflow distribution along the width of the SAH, with a low noise level and efficient energy consumption. Each blower has the

same dimensions and specifications as the other; it consumes 45 watts of electric power at the max speed. A conical galvanized steel sheet duct of a rectangular cross-section is fixed between the heating bed and the blower of each SAH. The steel duct is insulated using glass wool to reduce the heat losses to the ambient.

The MFR is controlled by two variacs (voltage regulators), one variac for each SAH. The variac manually changes the input voltage to the blower by a selector to get the desired flow rate. Each setup is supported by a steel perforated L-section stand and tilted 45°.

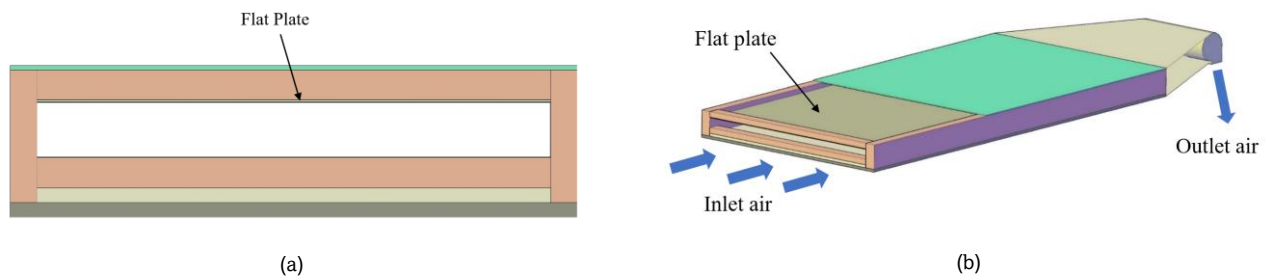


Fig 2. CAD of the FPSAH (a) Front view (b) ISO view

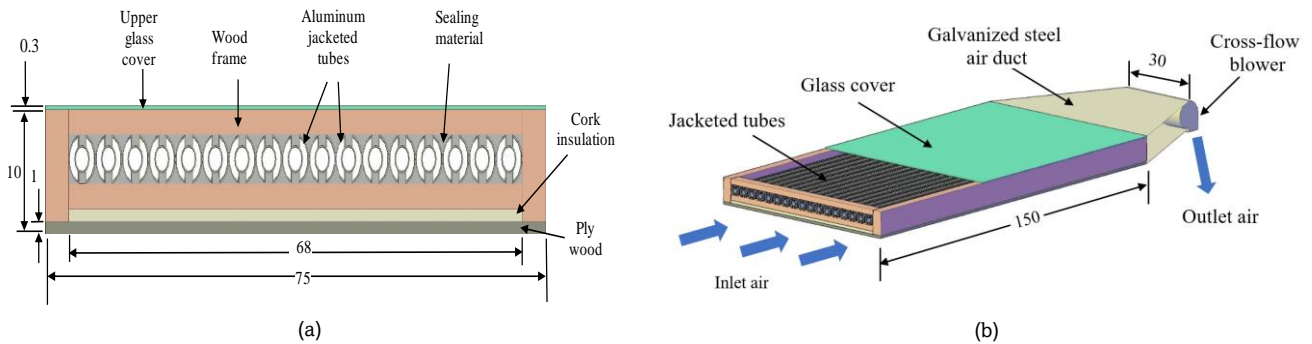


Fig 3. CAD of the JTSAH (a) Front view (b) ISO view



Fig 4. The absorbers of the SAHs: (a) FPSAH, (b) JTSAH

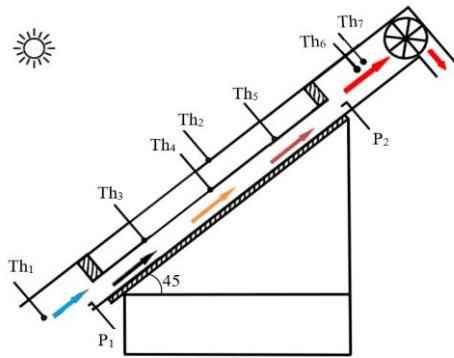


Fig 5. Positions of the temperature and pressure measuring points.

3 Measurement Points

Figure 5 shows the points where temperatures and pressures were measured. Temperature was measured using K-type thermocouples attached to the measurement points and connected to a temperature recorder Model: BTM-4208SD. The temperatures. Air temperatures at the inlet and outlet ports of each SAH were measured by one thermocouple mounted at the inlet section (Th₁), and two thermocouples (Th₆ and Th₇) mounted inside the duct to record the average outlet air temperature. The entering air temperature into each SAH is assumed to be equal to the ambient temperature. Three thermocouples are mounted along each SAH's absorber surface (Th₃, Th₄, Th₅) to calculate the average temperature of the plate (T_{plate}) or the tubes (T_{tube}). The glass cover temperature for each SAH was measured by one thermocouple mounted on its center (Th₂). All temperatures were measured and recorded.

The glass covers and absorber surface are too thin compared to the other two dimensions, so they are assumed to be infinite; the heat transfer is one-dimensional, and no temperature drops across their thicknesses occur. The pressure drop through each SAH was measured by a digital manometer that measures the differential total pressure between the points (P₁ and P₂).

Normal solar irradiation is measured by a solar power meter. An anemometer is used to measure the velocity of air. Experimental process and considerations

The temperatures and pressures had been measured and recorded for both of the SAHs from 8 A.M to 4 P.M on the days 26/11/ 2021, 27/11/2021, and 28/11/2021 at three MFRs of 0.011 kg/s, 0.033 kg/s, and 0.055 kg/s respectively.

The following experimental considerations were taken for each SAH in order:

- All of the thermocouples' points junction with the surfaces covered by an insulating adhesive Tape to improve the measurement and reduce the radiation effects.
- Before taking the measurements, the dust over the glass was cleaned with a cotton cloth.
- The instruments used in measuring the parameters were checked and calibrated, that includes. thermocouples, anemometer, solar power meter, manometer, voltmeter, ampere meter, temperature recorder, and also the sealing and insulations of the setup.
- The voltage was varied to get the required MFR.
- The required temperatures, MFR, and pressures were recorded during the experimentation.
- Temperature recording was recorded every 10 minutes automatically by the temperature recorder along with the duration between 8 AM and 4 PM.

- After finishing the test period of each day, the whole system preparation was set again (the cleaning procedure, checking the instruments, and preventing leaks.); getting ready for the next day of the test.

4 Data Reduction

The system's thermal efficiency (η_{th}) is calculated according to equation (1) (Zwalnan et al., 2021).

$$\eta_{th} = \frac{Q_{out}}{Q_{in}} \tag{1}$$

Where: Q_{out} is the gained thermal power of air out from the SAH, calculated according to equation (2) (Missoum & Loukarfi, 2021).

$$Q_{out} = MFR \times C_p \times \Delta T \tag{2}$$

It is required to calculate the mass flow rate of the passing air (MFR) calculated according to equation (3).

$$MFR = \rho \times V \times A_e \tag{3}$$

Where: $\rho = 1.225 \text{ kg/m}^3$; The density of air, assumed constant due to no high variation in the temperature and pressure, V : velocity of the air stream, measured by taking the average of five points at the outlet port, $A_e = (33.3 \text{ cm} \times 3.33 \text{ cm})$, The area of the outlet port, ΔT : (°C) The temperature difference of air (°C).

$$\Delta T = (T_{out} - T_{in}) \tag{4}$$

T_{in} : Temperature of air at the inlet (°C)
 T_{out} : Temperature of air at the outlet (°C)

Q_{in} is the incident solar power on the SAH absorber in W, and is calculated according to equation (5) (Olimat, 2017).

$$Q_{in} = I \times A_{abs} \tag{5}$$

Where, I , the normal solar irradiation on the absorber surface, $A_{abs} = (68 \text{ cm} \times 150 \text{ cm})$, The projected area of each absorber, is the same for both of them

The glass pane exchanges heat with the ambient and surrounding surfaces (Q_g), this heat is considered as the glass cover losses, calculated according to equation (6) (Kalogirou, 2014).

$$Q_{glass} = \frac{T_{glass} - T_{amb}}{\frac{1}{Ah_w + Ah_r}} \tag{6}$$

Where T_{glass} and T_{amb} are the glass and ambient air temperatures, h_w the convective heat transfer coefficient related to the wind, calculated according to equation (7) (Bouadila et al., 2013) and (Ansari & Bazargan, 2018).

$$h_w = 5.67 + 3.86V_w \tag{7}$$

Where V_w is the speed of the wind, neglected as it was too low during the days of the test, h_r is the radiative heat transfer coefficient of the same surface. Its value is calculated according to equation (8) (Kalogirou, 2014):

$$h_r = \frac{\sigma \varepsilon_g (T_{glass} + T_{sky})(T_{glass}^2 - T_{sky}^2)(T_{glass} - T_{sky})}{(T_{glass} - T_{amb})} \tag{8}$$

Where: ϵ_g : the emissivity of the glass material; assumed 0.9 (Kalogirou, 2014), σ : the Stefan Boltzmann constant, equals $5.667 \times 10^{-8} \text{ W/m}^2\text{K}$, T_{amb} and T_{sky} are the ambient (input port air) and sky temperatures.

When data for calculating the sky temperature are unavailable, the sky temperature may be calculated using the following equation from ISO 13790, calculated according to equation (9) (Asdrubali et al., 2019), considering Iraq as a tropical area.

$$T_{sky} = T_{amb} - 13 \tag{9}$$

The thermohydraulic efficiency η_{th-h} is calculated according to equation (10) (Priyam & Chand, 2016).

$$\eta_{th-h} = \frac{Q_{out} - W_{blower}}{Q_{in}} \tag{10}$$

Where W_{blower} is the electric power required to rotate the air blower

5 Results and Discussions

5.1 Temperature and solar irradiation

Temperature and solar irradiation were measured and recorded to investigate the two SAHs (FPSAH and J TSAH) thermal performance. The solar irradiation and temperatures were measured at MFR 0.011 kg/s are shown in Fig 6 (a) and (b). Likewise, the temperature and solar irradiation are recorded at MFR (0.033 kg/s) and demonstrated in Fig 7 (a) and (b). Furthermore, the last case of 0.055 kg/s MFR results is expressed in Fig 8 (a) and (b). The three figures show that the solar irradiation's intensity reaches its highest value at about 12:10 PM, and then declines. As we noted, there is not much variance in the solar radiation and ambient temperature for the experiment days. The figures revealed a close pattern of the temperatures as they escalate until about 12:30 PM when they start decreasing. At a higher absorber temperature, the air absorbs more heat, so the outlet air temperature increases. A time delay that takes place in the temperatures could be referred to as the stored energy in the SAH's material itself. The figures indicated that the maximum temperatures belong to the absorber (flat or tubular). The following high temperatures belong to the outlet and inlet air temperatures. Then comes the glass covers, respectively. These temperatures could be anticipated higher than the air temperature at the inlet. Table 1 abbreviates the maximum temperatures recorded during the experiment.

Table 1
The maximum temperatures measured for the FPSAH and J TSAH

MFR kg/s	Maximum Temperatures (°C)					
	FPSAH			J TSAH		
	T_{plate}	T_{glass}	T_{out}	T_{tube}	T_{glass}	T_{out}
0.011	77.1	39.1	54.9	64.2	35.3	61.2
0.033	61.6	34.5	39.3	49.8	31.0	43.9
0.055	54.9	31.6	33.7	44.2	28.6	37.4

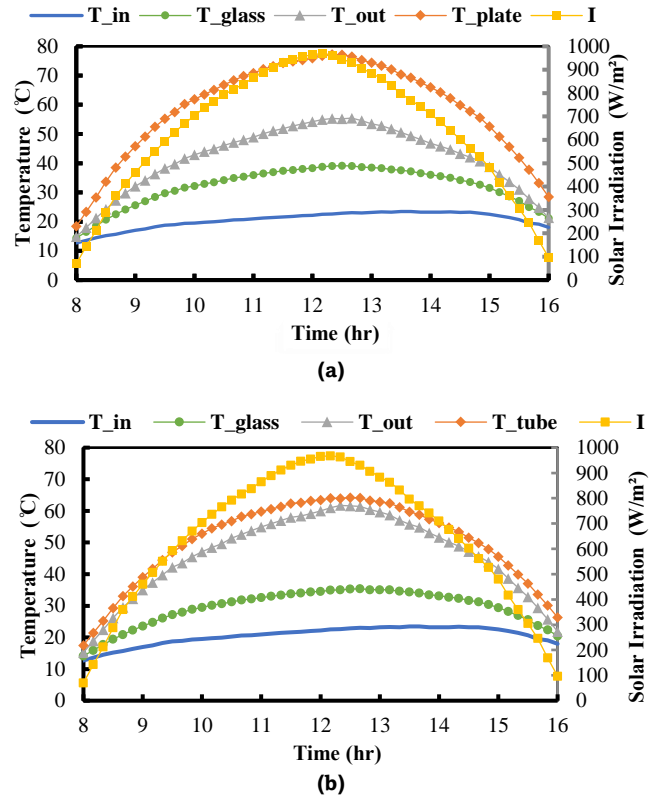


Fig 6. Variation of solar irradiation and temperature with time at MFR 0.011 kg/s with time for (a) FPSAH and (b) J TSAH.

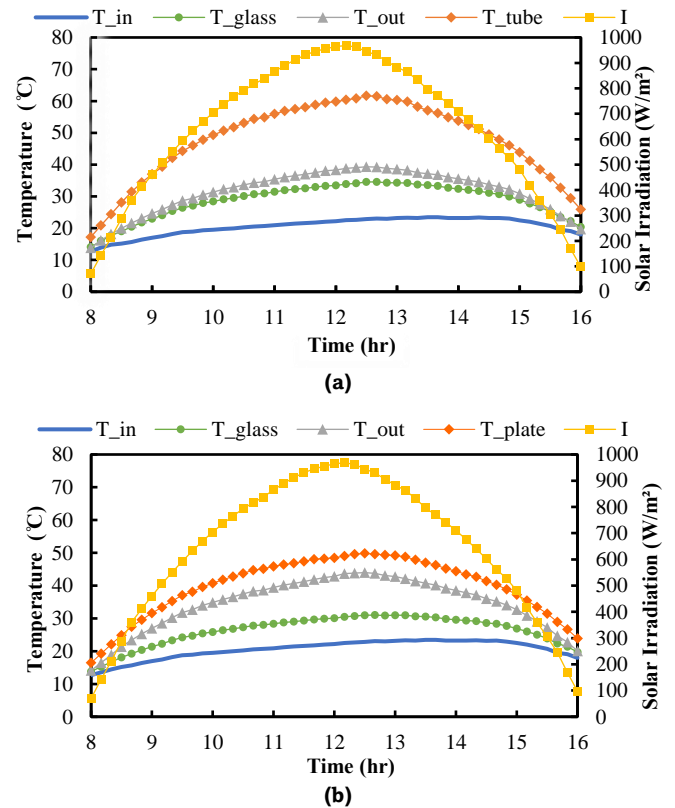


Fig 7. Variation of solar intensity and temperature with time MFR 0.033 kg/s with time for the (a) FPSAH and (b) J TSAH.

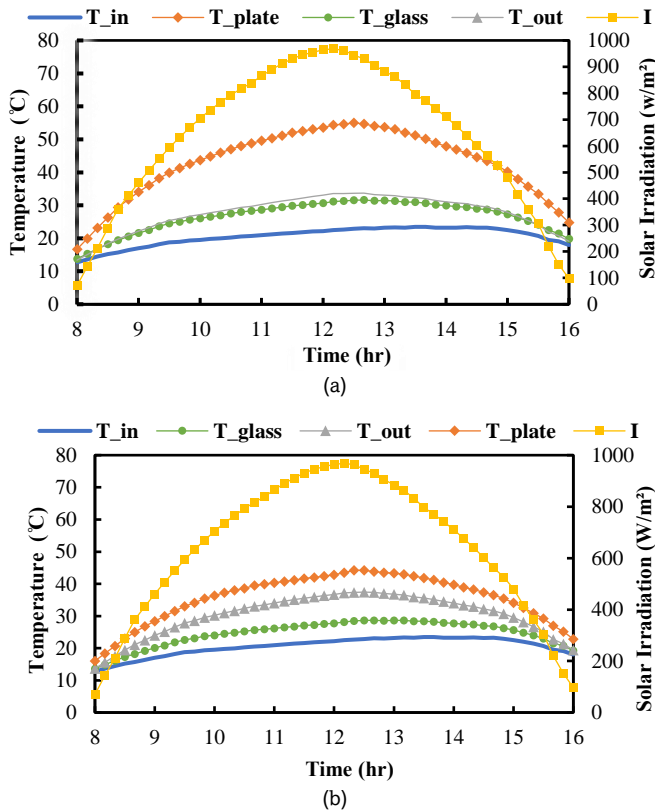


Fig 8. Variation of solar intensity and temperature with time at MFR 0.055 kg/s with time for the (a) FPSAH and (b) JTSAH.

The JTSAH’s lower absorber and glass temperature in comparison to the FPSAH is distinguishable, and vice-versa about the outlet air temperatures. The improvement in the T_{out} at the JTSAH in comparison to the FPSAH is 6.3°C, 4.6°C, 3.7°C at MFRs 0.011 kg/s, 0.033 kg/s, and 0.055 kg/s, respectively.

5.2 The Gained Power

Fig 9 (a), (b), and (c) establish the gained power (Q_{out}) in watts from the JTSAH and FPSAH at the three MFRs passed through each one. The gained power increases with the MFR due to reducing the absorber and the glass temperatures, which reduces the thermal losses. The gained power follows the same trend as the solar irradiation and temperatures; they rise throughout the day until the peak and then drop; This behavior belongs to the relation between the gained power and air temperature difference according to equation (2). The gained power from the JTSAH is higher than the FPSAH at the same MFR. The maximum gained power obtained was 814.3 W from the JTSAH at 0.055 kg/s MFR as shown in Fig 9 (c). The maximum enhancement in the gained power using JTSAH instead of the FPSAH is 105 W, 156 W, and 203 W, at 0.011 kg/s, 0.033 kg/s, and 0.055 kg/s MFRs respectively.

5.3 The accumulated energy

The accumulated energy ($Q_{out/accum.}$) from the SAHs represents the area under the gained power curves; it was calculated using the trapezoidal rule with 10 minutes (600 seconds) time step for each curve in the previous subsection. The accumulated energy values are in the megajoule unit (MJ) as demonstrated in Fig 10. The total accumulated energy increases with time from the beginning of recording until the finish of the experiment. Fig 10 demonstrates that the

accumulated energy from the JTSAH is higher in comparison to the FPSAH due to the improvement in the gained power of the JTSAH, also, they indicate that the power gained increases with increasing the MFR. The increment in the accumulated energy was 10.6 % when increased the MFR from 0.011 kg/s to 0.033 kg/s, and 6.3 % when the MFR increased from 0.033 kg/s to 0.055 kg/s.

5.4 Thermal Efficiency

The thermal efficiency of the SAH is calculated from equation (1). The evolution of the JTSAH and FPSAH thermal efficiencies at various airflow rates are revealed in Fig 11, which reveals that the SAH thermal efficiency varies with time from the morning until the end of the experiment time according to the parameters used in the calculation of efficiency.

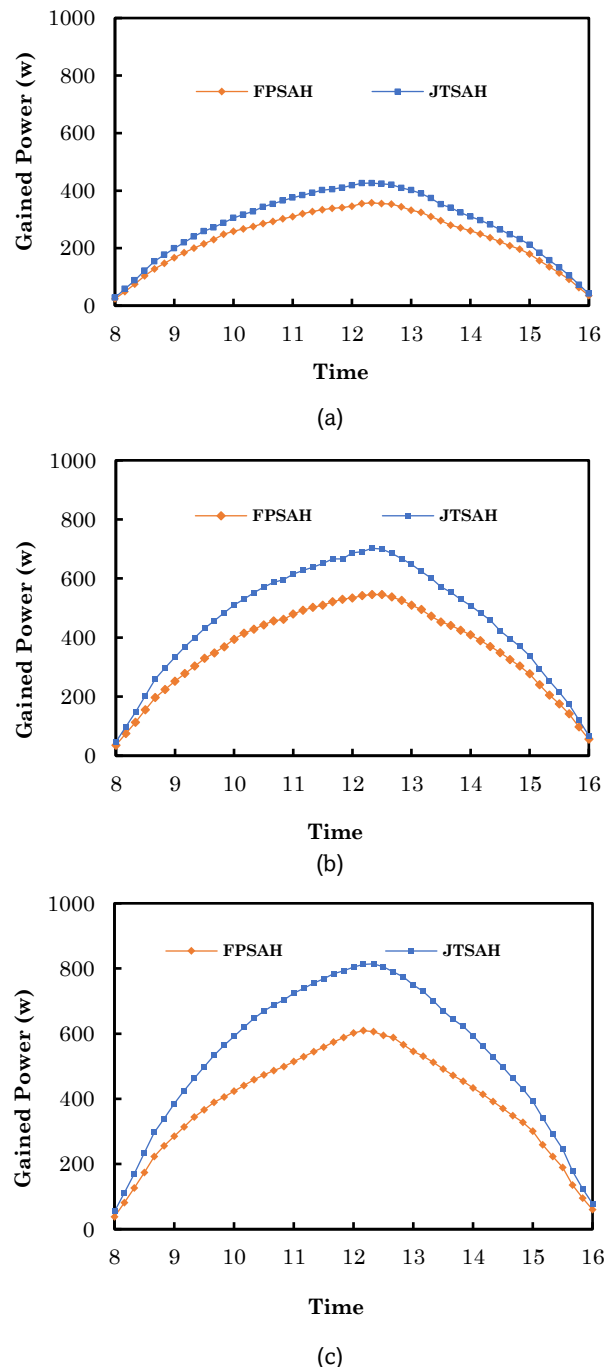


Fig 9. Gained Power profiles of the FPSAH and JTSAH at: (a)MFR = 0.011 kg/s, (b) MFR = 0.033 kg/s, (c) MFR = 0.055 kg/s.

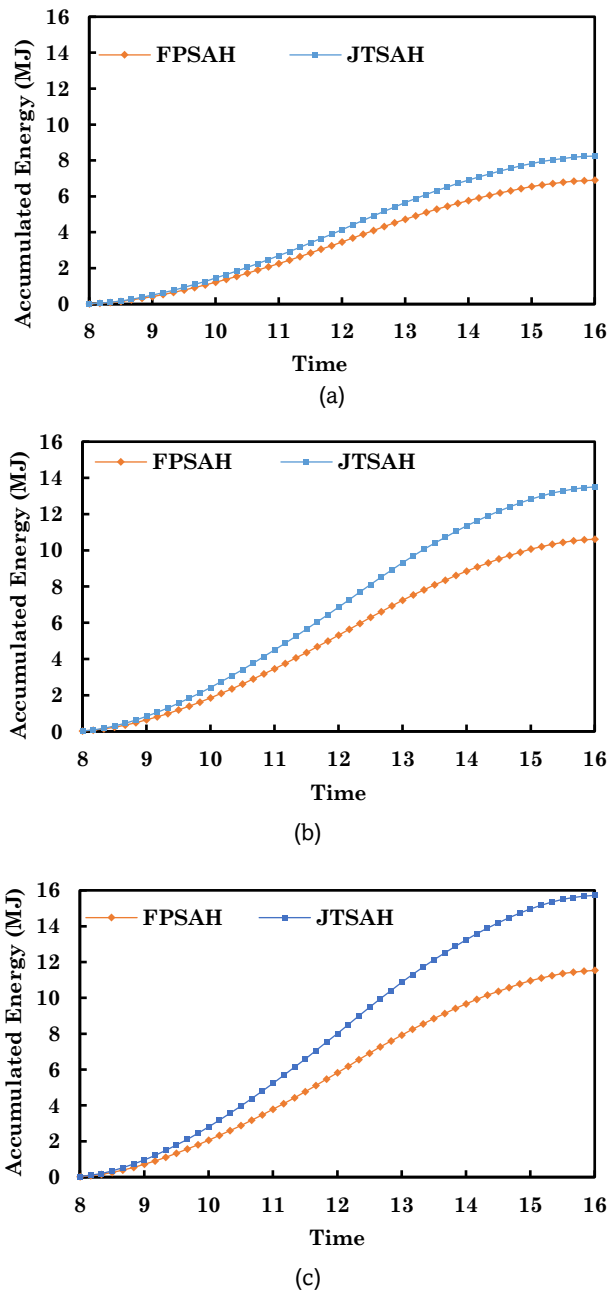


Fig 10. The accumulated energy of the FPSAH and J TSAH at:(a) MFR = 0.011 kg/s, (b) MFR = 0.033 kg/s, (c) MFR = 0.055 kg/s

During the early morning, some of the solar energy is stored in the SAH body, which could be the reason why the thermal efficiency is low at this period, then it increases with time as the solar irradiation becomes more normal on the absorber surface to reach its highest values between 12 noon and 1 PM, after that time, it decreases gradually till the end of the experiment. The amount of heat stored in the material of the SAH itself, the ambient temperature, and solar irradiation plays the role in the thermal efficiency curve behavior. The fluctuation in thermal efficiency curves is somewhat similar to other researches (Dabra *et al.*, 2013), (Singh & Vardhan, 2020), and (Khanlari *et al.*, 2020).

Fig 11 indicates that the thermal efficiency of the J TSAH for all studied MFRs is greater than the corresponding cases of the FSAH. Figure 13 shows that the maximum SAH efficiency reaches about 83.7 % in the case of J TSAH at MFRs 0.055 kg/s while this value is approximately 61.7 % for FPSAH under the

same circumstances, it is expected to get higher thermal efficiency if we run the blower to get MFR more than 0.055 kg/s due to the benefits gained at increasing the MFR. The average thermal efficiencies of the two studied SAHs at the specified MFRs with their increment are summarized in Table 4, which shows that the efficiency of the J TSAH is better than the matching flowrates of the FPSAH, the table also shows the increment in efficiency obtained from using the J TSAH instead of the FPSAH; it also increases as MFR increases. The increment in the average efficiency was 3 % when the MFR increased from 0.011 kg/s to 0.033 kg/s, and 12 % when the MFR was increased from 0.033 kg/s to 0.055 kg/s, which indicates the enhancement in thermal efficiency as the MFR increase.

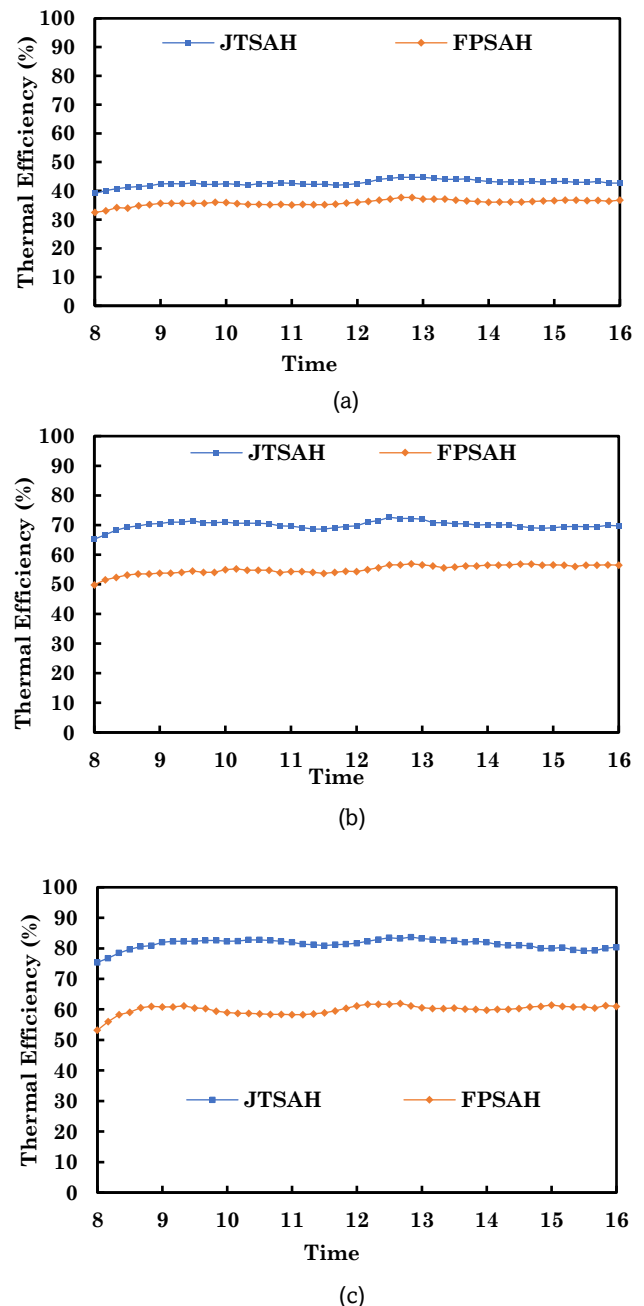


Fig 11. Instantaneous Efficiency of the FPSAH and J TSAH at: (a) MFR = 0.011 kg/s (b) MFR = 0.033 kg/s (c) MFR = 0.055 kg/s.

Table 2
Average thermal efficiencies obtained from previous researches

Reference	Absorber's design	Country or Region	Air Flow-Rate kg/s	Average thermal Efficiency %
(Khanlari et al., 2020)	U-tube DPSAH	Turkey	0.015	48.4
(Abdullah et al., 2018)	Flat plate with Aluminium cans	Saudi Arabia	0.05	68
(Hassan & Abo-Elfadl, 2018)	Corrugated Perforated Fins	Egypt	0.025	80
(Kabeel et al., 2018)	Flat finned plate	Egypt	0.04	57
(Nowzari et al., 2014)	Wire mesh	Turkey	0.032	55
(Jia et al., 2019)	Spiral spoiler	China	0.025	55
(I. Singh & Vardhan, 2020)	Evacuated Tube with Helical Inserts	India	0.015	52.88
(Iranmanesh et al., 2020)	Evacuated tube with thermal storage medium	Iran	0.09	55.57
(Dabra et al., 2013)	Evacuated tube with reflector	India	0.0037	61.02
The present research	JTSAH	Iraq	0.055	81.3

The enhancement in efficiency as a result of increasing the MFR in this research was also achieved by other previous researchers like (Kabeel et al., 2018), and (Nowzari et al., 2014). The average thermal efficiency of the JTSAH in this research was compared with the efficiencies of some published and reviewed previous designs in Table 2, which demonstrates various designs upon the SAH as trials to improve its efficiency like attaching turbulators, increasing the path of air inside the SAH, using tubular absorbers, adding spoilers. The JTSAH studied in this research is the most efficient among these researches at 0.055 kg/s MFR.

5.5 Thermohydraulic efficiency

The thermodynamic efficiency is used to evaluate the system's real thermal performance as it includes the air-blowing power considerations, so it is natural to be less than the thermal efficiency in value. Figure 12 shows the variation of the thermohydraulic efficiency with time. The thermohydraulic efficiency is primarily determined depending on the amount of heat gained, the irradiated solar irradiation on the absorber area, Moreover, by air pumping power, according to equation (10). It is noticeable that the highest thermohydraulic efficiency is obtained during the period confined between 12 noon and 1 PM due to the high gained power during this time. The highest thermohydraulic efficiency obtained from the experiment reaches 79.2% at the JTSAH at 0.055 kg/s MFR at 12:30 PM. The thermohydraulic efficiency is at its lowest values during the periods confined between 8 AM to 9 AM, and between 3 PM and 4 PM, the reason for this decrement is the low gained power from the solar irradiation, which protruded by the consumed electrical power by the blower. The electrical power needed for air to pass through the SAH for the three models are calculated experimentally, it is reasonable to note rise in electrical power consumed by the blowers as the MFR increase, also, at a specific MFR, this power is the least at the FPSAH, then increases at the JTSAH, the reason of this increment is the reduction in the air's cross-flow section inside the SAH' bed due to using tubes, this reduction resists the flowing of air causing more electrical losses.

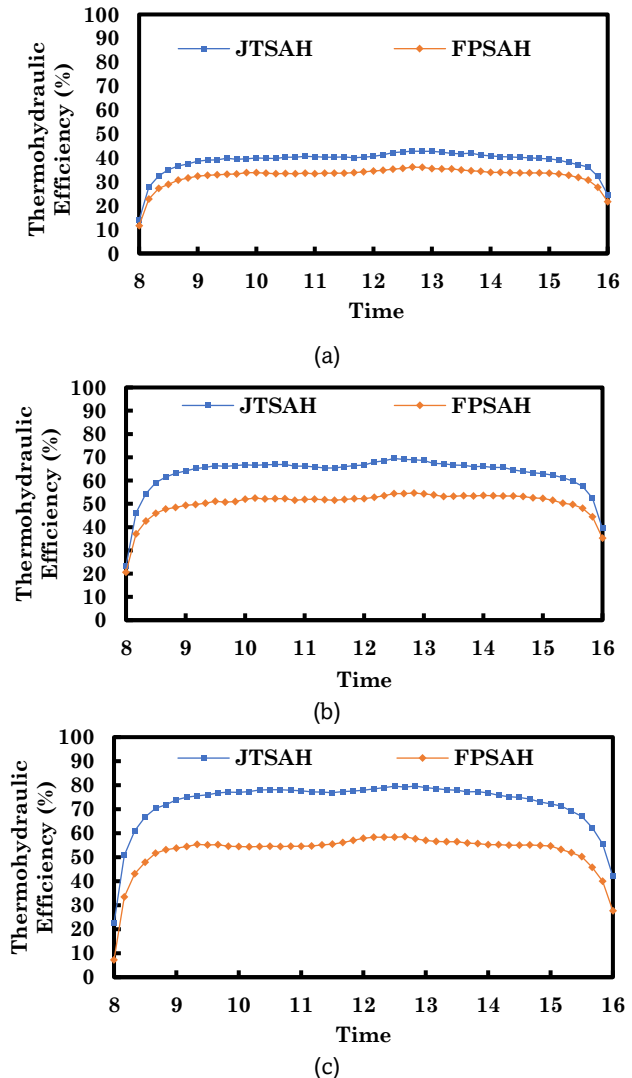


Fig 12 Instantaneous thermohydraulic efficiency of the FPSAH and JTSAH at: (a) MFR = 0.011 kg/s (b) MFR = 0.033 kg/s (c) MFR = 0.055 kg/s.

Table 3
Average thermohydraulic efficiencies obtained from previous researches

Reference	Absorber design	Country or Region	Air MFR (kg/s)	Average Thermos-hydraulic Efficiency %
(Chauhan & Thakur, 2014)	Flat plate + jet impinging	India	0.06	68
(Chand & Chand, 2018)	Finned Flat plate	India	0.06	70
(Priyam & Chand, 2016)	Wavy channel + wavy fins	India	0.08	72
(Rai et al., 2018)	Finned Flat plate	India	0.04	77
The Presented research	JTSAH	Iraq	0.055	79.5

Table 4
Comprehensive calculated values in the presented research.

MFR kg/s	Total $Q_{out/accum.}$ (MJ)		Average thermal efficiency (%)			Blower Electrical Power (watts)		Average thermohydraulic efficiency (%)		
	FPSAH	JTSAH	FPSAH	JTSAH	Increment percentage (%)	FPSAH	JTSAH	FPSAH	JTSAH	Increment percentage (%)
0.011	6.9	8.24	35.88	42.7	20	15	18	32.46	38.65	19.07
0.033	10.61	13.5	55.04	68.1	23	21	30	48.26	63.16	30.8
0.055	11.53	15.72	59.5	81.3	35	30	42	54.33	75.61	39.16

The average thermohydraulic efficiency is smaller than thermal efficiency, because of the electricity consumed, and taken into account, the table also shows that the SAHs' average thermohydraulic efficiency improves as the MFR of the entering air increase. The enhancement in thermohydraulic efficiency as a function of increasing the MFR in this research has a behavior similar to other previous researchers as (Rai et al., 2018), and (Priyam & Chand, 2016). Table 3 reviews the average thermohydraulic efficiencies obtained from previous researches with their air MFRs, it shows the high thermohydraulic efficiency obtained from this research at the JTSAH at 0.055 kg/s MFR in comparison to the other researches Table 4 shows that the average thermal and thermal efficiencies of the JTSAH are better than the matching flow rates at the FPSAH with their increment percentages, the Table also shows the increment in efficiency obtained from using the JTSAH instead of the FPSAH; it also increases as MFR increases. indicates the enhancement in thermal efficiency as the MFR increase.

5.6. Glass Cover Losses

Thermal losses follows the process of heat transfer through the SAH. Energy is lost from the absorber, the glass, the frame, and other parts. Our research investigated the losses from the glass cover particularly. The thermal power lost from the glass cover (Q_{glass}) by convection and radiation as a result of its high temperature in comparison to the surroundings and ambient air was calculated according to equation (6). The glass cover losses are better to be minimized because they reduce the performance of the system. The glass cover losses changes with time and the MFR as shown in Fig 12 (a), (b), and (c), depending on the temperature of the glass mainly, and could be reduced by reducing the glass cover temperature. The glass cover losses in the case of the FPSAH are larger than the JTSAH's due to the higher glass temperature.

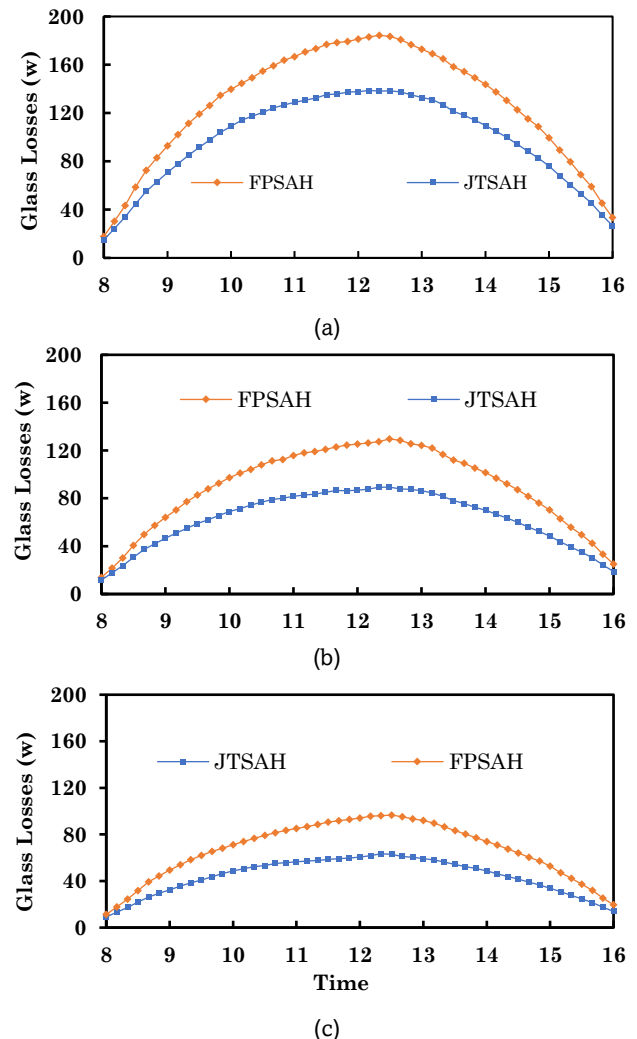


Fig 12. Glass Cover Losses of the FPSAH and JTSAH at: (a) MFR= 0.011 kg/s, (b) MFR = 0.033 kg/s, (c) MFR = 0.055 kg/s.

Table 5
The Impact of MFR on the SAHs pressure drop

MFR	Pressure Drop (Pa)		Increment percentage (%)
	FPSAH	JTSAH	
0.011	12	15	25
0.033	17	24	39
0.055	22	40	53

5.7 Pressure drops

Pressure drop through the SAH takes part as the SAH resists the flowing air, increases the power required to run the blower, and increases the operating costs of the SAH. In the SAH, the energy gain and heat transfer were enhanced by using a jacketed tubes absorber, this enhancement is accompanied by an increased pressure drop through the flow channel along the axial direction of the collector as a disadvantage of using the modified absorber. The airflow can be assumed uniform in the distribution through all of the pipes. Table 5 shows the pressure drop value at each MFR in the experimental part for the FPSAH, and JTSAH. The pressure drop increment at the JTSAH compared to the FPSAH increased 14% when MFR increased from 0.011 kg/s to 0.033 kg/s, it also increased 14% when MFR increased from 0.033 kg/s to 0.055 kg/s. In the case of JTSAH, the pressure decrease is noticeably more remarkable than in the case of FPSAH due to the higher drag between the tubes and air. The pressure drop through the modified absorber in this paper (JTSAH) is low in comparison to other absorbers as finned (Rai *et al.*, 2018), louvered (Chand & Chand, 2018), tubular (Hassan *et al.*, 2020), ribbed absorbers (Wang *et al.*, 2020). This decrement considered an enhancement in reducing the power consumption of air blowing apparatus.

6 Conclusion

The JTSAH has higher thermal and thermohydraulic efficiencies at any specific MFR in comparison to the FPSAH, contrarily, The JTSAH has lower thermal losses in comparison to the FPSAH, the reason beyond this variation is the larger contact area between the flowing air and absorber of the jacketed tube, which is 6.28 times the flat plate area, furthermore, the area exposed to solar radiation in the JTASH's absorber is 1.5 times the same area of the FPSAH's absorber; Another benefit of using this tubular absorber is the reflection of some solar rays between the tubes. The used jacketed-tube absorber increases the heat transfer between the tubes and air at the JTSAH. Increasing the MFR increases the thermal and thermohydraulic efficiencies, because it reduces the absorber temperature, enhancing the heat transfer through the absorber. Increasing the MFR enhances thermohydraulic efficiency. The pressure drop through the JTSAH is higher than the FPSAH due to its large contact area with air, this drop is opposed by an enhancement in the thermohydraulic efficiency. The JTSAH in this research has been also compared with some previous research, it showed an increment in thermal and thermohydraulic efficiencies, utilizing two glass covers rather than one.

Some recommendations may be the focus of future research upon the recent one, like attaching a drying chamber for agricultural drying, employing porous media inside the SAH to improve the efficiency, utilizing two glass covers rather than one, and attaching PCM containers to store energy, and else.

References

Abdullah, A. S., Abou Al-sood, M. M., Omara, Z. M., Bek, M. A., & Kabeel,

- A. E. (2018). Performance evaluation of a new counter flow double pass solar air heater with turbulators. *Solar Energy*, 173(July), 398–406. <https://doi.org/10.1016/j.solener.2018.07.073>
- Abdullah, A. S., El-Samadony, Y. A. F., & Omara, Z. M. (2017). Performance evaluation of plastic solar air heater with different cross sectional configuration. *Applied Thermal Engineering*, 121, 218–223. <https://doi.org/10.1016/j.applthermaleng.2017.04.067>
- Aboghrara, A. M., Baharudin, B. T. H. T., Alghoul, M. A., Adam, N. M., Hairuddin, A. A., & Hasan, H. A. (2017). Performance analysis of solar air heater with jet impingement on corrugated absorber plate. *Case Studies in Thermal Engineering*, 10, 111–120. <https://doi.org/10.1016/j.csite.2017.04.002>
- Ansari, M., & Bazargan, M. (2018). Optimization of flat plate solar air heaters with ribbed surfaces. *Applied Thermal Engineering*, 136(February), 356–363. <https://doi.org/10.1016/j.applthermaleng.2018.02.099>
- Arunkumar, H. S., Vasudeva Karanth, K., & Kumar, S. (2020). Review on the design modifications of a solar air heater for improvement in the thermal performance. *Sustainable Energy Technologies and Assessments*, 39(March), 100685. <https://doi.org/10.1016/j.seta.2020.100685>
- Bakry, A. I., El-Samadouny, Y. A. F., El-Agouz, S. A., Alshrombably, A. M., Abdelfatah, K. S., & Said, M. A. (2018). Performance of the one-ended evacuated tubes as medium temperature solar air heaters at low flow rates. *Sustainable Energy Technologies and Assessments*, 30(October), 174–182. <https://doi.org/10.1016/j.seta.2018.10.002>
- Bensaci, C. E., Moumami, A., Sanchez de la Flor, F. J., Rodriguez Jara, E. A., Rincon-Casado, A., & Ruiz-Pardo, A. (2020). Numerical and experimental study of the heat transfer and hydraulic performance of solar air heaters with different baffle positions. *Renewable Energy*, 155, 1231–1244. <https://doi.org/10.1016/j.renene.2020.04.017>
- Bouadila, S., Kooli, S., Lazaar, M., Skouri, S., & Farhat, A. (2013). Performance of a new solar air heater with packed-bed latent storage energy for nocturnal use. *Applied Energy*, 110, 267–275. <https://doi.org/10.1016/j.apenergy.2013.04.062>
- Chabane, F., Moumami, N., & Benramache, S. (2014). Experimental study of heat transfer and thermal performance with longitudinal fins of solar air heater. *Journal of Advanced Research*, 5(2), 183–192. <https://doi.org/10.1016/j.jare.2013.03.001>
- Chand, S., & Chand, P. (2018). Parametric study on the performance of solar air heater equipped with louvered fins. *Journal of Mechanical Science and Technology*, 32(8), 3965–3973. <https://doi.org/10.1007/s12206-018-0747-y>
- Chauhan, R., & Thakur, N. S. (2014). Investigation of the thermohydraulic performance of impinging jet solar air heater. *Energy*, 68, 255–261. <https://doi.org/10.1016/j.energy.2014.02.059>
- Dabra, V., Yadav, L., & Yadav, A. (2013). The effect of tilt angle on the performance of evacuated tube solar air collector: experimental analysis. 5(4), 100–110.
- Dissa, A. O., Ouoba, S., Bathiebo, D., & Koulidiati, J. (2016). A study of a solar air collector with a mixed “porous” and “non-porous” composite absorber. *Solar Energy*, 129, 156–174. <https://doi.org/10.1016/j.solener.2016.01.048>
- Fiuk, J. J., & Dutkowski, K. (2019). Experimental investigations on thermal efficiency of a prototype passive solar air collector with wavelike baffles. *Solar Energy*, 188(June), 495–506. <https://doi.org/10.1016/j.solener.2019.06.030>
- Ghritlahre, H. K., Sahu, P. K., & Chand, S. (2020). Thermal performance and heat transfer analysis of arc shaped roughened solar air heater – An experimental study. *Solar Energy*, 199(December 2019), 173–182. <https://doi.org/10.1016/j.solener.2020.01.068>
- Hassan, H., & Abo-Elfadl, S. (2018). Experimental study on the performance of double pass and two inlet ports solar air heater (SAH) at different configurations of the absorber plate. *Renewable Energy*, 116, 728–740. <https://doi.org/10.1016/j.renene.2017.09.047>
- Hassan, H., Abo-Elfadl, S., & El-Dosoky, M. F. (2020). An experimental investigation of the performance of new design of solar air heater (tubular). *Renewable Energy*, 151, 1055–1066. <https://doi.org/10.1016/j.renene.2019.11.112>
- Heydari, A., & Mesgarpour, M. (2018). Experimental analysis and numerical modeling of solar air heater with helical flow path. *Solar*

- Energy*, 162(November 2017), 278–288. <https://doi.org/10.1016/j.solener.2018.01.030>
- Hosseini, S. S., Ramiar, A., & Ranjbar, A. A. (2019). The effect of fins shadow on natural convection solar air heater. *International Journal of Thermal Sciences*, 142(May), 280–294. <https://doi.org/10.1016/j.ijthermalsci.2019.04.015>
- Iranmanesh, M., Samimi Akhijahani, H., & Barghi Jahromi, M. S. (2020). CFD modeling and evaluation the performance of a solar cabinet dryer equipped with evacuated tube solar collector and thermal storage system. *Renewable Energy*, 145, 1192–1213. <https://doi.org/10.1016/j.renene.2019.06.038>
- Jia, B., Liu, F., & Wang, D. (2019). Experimental study on the performance of spiral solar air heater. *Solar Energy*, 182(February), 16–21. <https://doi.org/10.1016/j.solener.2019.02.033>
- Jouybari, N. F., & Lundström, T. S. (2020). Performance improvement of a solar air heater by covering the absorber plate with a thin porous material. *Energy*, 190. <https://doi.org/10.1016/j.energy.2019.116437>
- Kabeel, A. E., Hamed, M. H., Omara, Z. M., & Kandeal, A. W. (2018). Influence of fin height on the performance of a glazed and bladed entrance single-pass solar air heater. *Solar Energy*, 162(September 2017), 410–419. <https://doi.org/10.1016/j.solener.2018.01.037>
- Kalaiarasi, G., Velraj, R., Vanjeswaran, M. N., & Ganesh Pandian, N. (2020). Experimental analysis and comparison of flat plate solar air heater with and without integrated sensible heat storage. *Renewable Energy*, 150, 255–265. <https://doi.org/10.1016/j.renene.2019.12.116>
- Kalogirou, S. A. (2014). Solar Energy Engineering: Processes and Systems: Second Edition. In *Solar Energy Engineering: Processes and Systems: Second Edition*. <https://doi.org/10.1016/C2011-0-07038-2>
- Khanlari, A., Sözen, A., Şirin, C., Tuncer, A. D., & Gungor, A. (2020). Performance enhancement of a greenhouse dryer: Analysis of a cost-effective alternative solar air heater. *Journal of Cleaner Production*, 119672. <https://doi.org/10.1016/j.jclepro.2019.119672>
- Komolafe, C. A., Oluwaleye, I. O., Awogbemi, O., & Osuke, C. O. (2019). Experimental investigation and thermal analysis of solar air heater having rectangular rib roughness on the absorber plate. *Case Studies in Thermal Engineering*, 14(March). <https://doi.org/10.1016/j.csite.2019.100442>
- Missoum, M., & Loukarfi, L. (2021). Investigation of a solar polygeneration system for a multi-storey residential building-dynamic simulation and performance analysis IJRED. *International Journal of Renewable Energy Development*, 10(3), 445–458. <https://doi.org/10.14710/ijred.2021.34423>
- Murali, G., Sundari, A. T. M., Raviteja, S., Chanukyachakravarthi, S., & Tejpraneeth, M. (2020). Experimental study of thermal performance of solar aluminium cane air heater with and without fins. *Materials Today: Proceedings*, 21, 223–230. <https://doi.org/10.1016/j.matpr.2019.04.224>
- Nidhul, K., Kumar, S., Yadav, A. K., & Anish, S. (2020). Enhanced thermo-hydraulic performance in a V-ribbed triangular duct solar air heater: CFD and exergy analysis. *Energy*, 200, 117448. <https://doi.org/10.1016/j.energy.2020.117448>
- Nowzari, R., Aldabbagh, L. B. Y., & Egelioglu, F. (2014). Single and double pass solar air heaters with partially perforated cover and packed mesh. *Energy*, 73, 694–702. <https://doi.org/10.1016/j.energy.2014.06.069>
- Olimat, A. N. (2017). Study of fabricated solar dryer of tomato slices under Jordan climate condition IJRED. *International Journal of Renewable Energy Development*, 6(2), 93–101. <https://doi.org/10.14710/ijred.6.2.93-101>
- Priyam, A., & Chand, P. (2016). Thermal and thermohydraulic performance of wavy finned absorber solar air heater. *Solar Energy*, 130, 250–259. <https://doi.org/10.1016/j.solener.2016.02.030>
- Rai, S., Chand, P., & Sharma, S. P. (2018). Evaluation of thermo hydraulic effect on offset finned absorber solar air heater. *Renewable Energy*, 125, 39–54. <https://doi.org/10.1016/j.renene.2018.01.110>
- Ravi, R. K., & Saini, R. P. (2016). Experimental investigation on performance of a double pass artificial roughened solar air heater duct having roughness elements of the combination of discrete multi V shaped and staggered ribs. *Energy*, 116, 507–516. <https://doi.org/10.1016/j.energy.2016.09.138>
- Saravanakumar, P. T., Somasundaram, D., & Matheswaran, M. M. (2019). Thermal and thermo-hydraulic analysis of arc shaped rib roughened solar air heater integrated with fins and baffles. *Solar Energy*, 180(January), 360–371. <https://doi.org/10.1016/j.solener.2019.01.036>
- Shetty, S. P., Paineni, A., Kande, M., Madhwesh, N., Yagnesh Sharma, N., & Vasudeva Karanth, K. (2020). Experimental investigations on a cross flow solar air heater having perforated circular absorber plate for thermal performance augmentation. *Solar Energy*, 197(August 2019), 254–265. <https://doi.org/10.1016/j.solener.2020.01.005>
- Singh, A. P., & Singh, O. P. (2018). Performance enhancement of a curved solar air heater using CFD. *Solar Energy*, 174(April), 556–569. <https://doi.org/10.1016/j.solener.2018.09.053>
- Singh, I., & Vardhan, S. (2020). Experimental Investigation of an Evacuated Tube Collector Solar Air Heater with Helical Inserts. *Renewable Energy*. <https://doi.org/10.1016/j.renene.2020.10.114>
- Singh Patel, S., & Lanjewar, A. (2019). Experimental and numerical investigation of solar air heater with novel V-rib geometry. *Journal of Energy Storage*, 21(January), 750–764. <https://doi.org/10.1016/j.est.2019.01.016>
- Singh, S. (2020). Experimental and numerical investigations of a single and double pass porous serpentine wavy wiremesh packed bed solar air heater. *Renewable Energy*, 145, 1361–1387. <https://doi.org/10.1016/j.renene.2019.06.137>
- Sivakandhan, C., Arjunan, T. V., & Matheswaran, M. M. (2020). Thermohydraulic performance enhancement of a new hybrid duct solar air heater with inclined rib roughness. *Renewable Energy*, 147, 2345–2357. <https://doi.org/10.1016/j.renene.2019.10.007>
- Soares, N. (2015). Thermal energy storage with phase change materials (PCMs) for the improvement of the Energy performance of buildings. PhD Thesis. Sustainable Energy Systems. Department of Mechanical Engineering - UNIVERSITY OF COIMBRA, 2015. *Renewable and Sustainable Energy Reviews*, 80.
- Thakur, D. S., Khan, M. K., & Pathak, M. (2017). Performance evaluation of solar air heater with novel hyperbolic rib geometry. *Renewable Energy*, 105, 786–797. <https://doi.org/10.1016/j.renene.2016.12.092>
- Wang, D., Gao, Q., Liu, Y., Wang, Y., Chen, Y., Liu, Y., & Liu, J. (2019). Experimental study on heating characteristics and parameter optimization of transpired solar collectors. *Applied Energy*, 238(January), 534–546. <https://doi.org/10.1016/j.apenergy.2019.01.004>
- Wang, D., Liu, J. J., Liu, Y., Wang, Y., Li, B., & Liu, J. J. (2020). Evaluation of the performance of an improved solar air heater with “S” shaped ribs with gap. *Solar Energy*, 195(13), 89–101. <https://doi.org/10.1016/j.solener.2019.11.034>
- Wang, Z., Diao, Y., Zhao, Y., Chen, C., Liang, L., & Wang, T. (2020). Thermal performance of integrated collector storage solar air heater with evacuated tube and lap joint-type fl at micro-heat pipe arrays. *Applied Energy*, 261(September 2019), 114466. <https://doi.org/10.1016/j.apenergy.2019.114466>
- Yagnesh Sharma, N., Madhwesh, N., & Vasudeva Karanth, K. (2019). The effect of flow obstacles of different shapes for generating turbulent flow for improved performance of the solar air heater. *Procedia Manufacturing*, 35, 1096–1101. <https://doi.org/10.1016/j.promfg.2019.06.062>
- Zukowski, M. (2015). Experimental investigations of thermal and flow characteristics of a novel microjet air solar heater. *Applied Energy*, 142, 10–20. <https://doi.org/10.1016/j.apenergy.2014.12.052>
- Zwalnan, S. J., Duvuna, G. A., Abakr, Y. A., & Banda, T. (2021). Design and performance evaluation of a multi-temperature flat plate solar collector IJRED. *International Journal of Renewable Energy Development*, 10(3), 537–549. <https://doi.org/10.14710/ijred.2021.33213>

